Biomass and Bioenergy 193 (2025) 107574

Contents lists available at ScienceDirect

Biomass and Bioenergy

journal homepage: www.elsevier.com/locate/biombioe

Evaluating the impact of pre-carbonization on activated carbon production from animal-origin precursors for supercapacitor electrode applications

Diego Ramón Lobato-Peralta [a,*], Jude A. Okolie [b], Henry O. Orugba [c], D.M. Arias [d], P.J. Sebastian [d], Patrick U. Okoye [d,**]

[a] Instituto de Carboquímica, CSIC, Miguel Luesma Castán 4, Zaragoga, 50018, Spain
[b] Department of chemical Engineering-Bucknell University, One Dent Drive, Lewisburg, PA, 17837, United States
[c] Department of Chemical and Petroleum Engineering, Delta State University, Abraka, Oleh Campus, P.M.B. 22, Oleh, Nigeria
[d] Instituto de Energías Renovables, Universidad Nacional Autónoma de México, Privada Xochicalco S/N, Col. Centro, Temixco, 62580, Mexico

ARTICLE INFO

Keywords:
Biomass pyrolysis
Chemical carbon activation
Supercapacitors
Pig processing
Electrochemical energy storage
Carbon-based electrode

ABSTRACT

This study investigates the effect of pre-carbonization temperature on the energy storage properties of activated carbons derived from animal-origin precursors, specifically for application as supercapacitor electrodes. The objective was to develop materials with enhanced electrochemical performance. Pig hair, an abundant and sustainable carbon source, was utilized to synthesize a series of carbons with hierarchical porosity. The process involved pre-carbonization at temperatures of 350, 400, 450, and 500 °C, followed by chemical activation at 800 °C using potassium hydroxide (KOH) at a biomass-to-KOH ratio of 1:3. The resulting carbons exhibited a disordered morphology with a high surface area, reaching up to 1002 m^2/g, predominantly composed of micro- and mesopores. These structural features facilitated energy storage primarily through electric double-layer capacitance rather than faradaic processes. Detailed electrochemical testing revealed a clear dependence on pre-carbonization temperature, with electrode performance ranking in the order of 500 °C > 450 °C > 350 °C > 400 °C. This work underscores the critical role of pre-carbonization temperature in tailoring the structural and electrochemical properties of activated carbons derived from animal-based precursors. By systematically exploring this parameter, the study provides valuable insights into the design of sustainable, high-performance materials for energy storage, contributing to the broader development of eco-friendly energy solutions.

1. Introduction

Supercapacitors, sometimes referred to as electrochemical capacitors, are cutting-edge energy storage devices that are gaining traction due to their unique ability to bridge the gap between traditional capacitors and batteries [1]. These devices are known for their exceptional power density, rapid charging and discharging capabilities, and long lifespan, making them highly suitable for diverse applications ranging from portable electronics to electric vehicles and renewable energy systems [2]. As the world moves towards more sustainable energy solutions, supercapacitors are emerging as a vital technology to address some of the limitations associated with conventional energy storage options. Supercapacitors are increasingly recognized for their sustainable nature, especially when compared to traditional batteries. While conventional batteries often rely on scarce and environmentally damaging materials such as cobalt and lithium, supercapacitors can be made from more abundant and eco-friendly alternatives, like carbon-based electrodes [3,4]. Moreover, the extended cycle life of supercapacitors, often exceeding one million charge-discharge cycles, minimizes the frequency of replacements, thus reducing electronic waste.

A supercapacitor consists of two electrodes immersed in an electrolyte and separated by a membrane. The performance of the device is highly influenced by the cell design, as well as the quality and characteristics of the electrodes, which are responsible for storing and releasing charge as needed [5]. Consequently, numerous researchers have investigated various materials for electrode production, including metal oxides, conducting polymers, carbon nanotubes, graphene, and activated carbon which is an abundant and eco-friendly alternative.

The primary mechanism of energy storage in carbon materials is

* Corresponding author.
** Corresponding author.
E-mail addresses: dlobato@icb.csic.es (D.R. Lobato-Peralta), ugopaok@ier.unam.mx (P.U. Okoye).

https://doi.org/10.1016/j.biombioe.2024.107574
Received 8 October 2024; Received in revised form 4 December 2024; Accepted 23 December 2024
Available online 31 December 2024

through the electric double layer, which depends on charge separation at the interface between the electrode and electrolyte. This physical process necessitates the transport of ions into and out of the electrode. Therefore, a significantly large surface area is essential to facilitate ion transport and provide sufficient storage sites for ions generated from the electrolyte when voltage is applied to the electrodes [6].

Activated carbon materials possess essential properties, including a large surface area that facilitates ion mobility and electron transfer. These properties are developed through a process called activation, which creates pores on the material's surface. Activation can be achieved through various methods, including physical activation (using oxidizing gases such as CO_2, steam, or oxygen) and chemical activation, which involves impregnating the precursor with activating agents. It is important to note that not all activation processes produce materials with the same characteristics, for instance, Barakat et al. [7] compared two activated carbons produced through chemical activation with phosphoric acid and potassium hydroxide. Also, they investigated single step and two-step activation process to obtain activated carbon. They reported 18 % increase in stability over a 1000 charge/discharge cycle compared to the alkali activated carbon. This trend was also observed with the capacitance of the materials, however, due to lower surface area, the capacitance was around 88.5 F/g for scan rate of 2 mV/s. Another study that used corncob and phosphoric acid to produce activated carbon for supercapacitor electrode obtained very low surface area and consequent low capacitance of 41 F/g. Their device retained 88 % capacitance over 2000 charge/discharge cycles at 10 A/g [8].

Furthermore, hemp fiber has been treated hydrothermally to remove the cellulose content and then activated using KOH to obtain activated carbon with characteristically high surface area. This material produced a capacitance of 255.1 F/g at current density of 1 A/g in a three-electrode system. The capacitance retention was 102 % in 10,000 cycles of charge/discharge with maximum power density of 75 W/kg [9]. Another interesting recent study used *Mesua ferrea* shell (a shell usually found in south India) with deep eutectic salts to produce activated carbon. They remarked that activation temperature significantly influenced the nitrogen content, structure and surface area of the carbon. At 700 °C (BET: 570.917 m^2/g), they realized a capacitance of 210 F/g, which is about 8 times higher than the capacitance of the sample produced at 800 °C (BET: 250.798 m^2/g) [10]. Among all the chemical activating agents, KOH has proven to be an excellent activating agent due to the reactions it carries out with the precursors, which result in highly developed porosity. These reactions are presented in Equations (1)–(6) [11]:

$$6KOH + 2C \rightarrow 2K + 2H_2 + 2K_2CO_3 \quad (1)$$

$$6KOH + 3CO_2 \rightarrow 3K_2CO_3 + 3H_2O \quad (2)$$

$$K_2CO_3 \rightarrow K_2O + CO_2 \quad (3)$$

$$CO_2 + C \rightarrow 2CO \quad (4)$$

$$K_2CO_3 + C \rightarrow 2K + 3CO \quad (5)$$

$$K_2O + C \rightarrow 2K + CO \quad (6)$$

In which respects to precursors, activated carbon can be produced from waste materials, reducing production costs and promoting a circular bioeconomy. These waste sources can vary, including agricultural byproducts such as rice husk [12], agave leaves [13], rubber leaves [14], and others. Agricultural residues have emerged as a prominent resource for producing activated carbon for supercapacitor electrodes. These materials not only offer widespread availability but also present several compelling advantages. Converting biomass into carbon materials provides an indirect approach to utilizing CO_2 as a carbon feedstock, promoting the development of sustainable energy storage technologies while simultaneously contributing to pollution mitigation. In recent years, the demand for eco-friendly and sustainable materials has significantly increased, elevating the popularity of biomass-derived carbons. These materials are economically viable, environmentally sustainable, and rich in carbon content. They also demonstrate excellent electrical conductivity and exceptional physicochemical properties. Importantly, the distinctive structures of these carbon materials enhance their ability to facilitate the efficient transport of electrolyte ions within the electrodes, making them highly suitable for energy storage applications [15–17].

Activated carbon materials offer several advantages as electrodes for supercapacitors compared to pure metal oxides, metal-organic frameworks (MOFs), covalent organic frameworks (COFs), and conducting polymers. Their high surface area and hierarchical pore structures provide abundant sites for charge storage via electric double-layer capacitance, ensuring rapid ion transport and high-power density. Unlike pure metal oxides, which primarily rely on faradaic processes and can suffer from limited cycle life due to structural degradation, activated carbons exhibit excellent stability and durability over prolonged charge-discharge cycles. They are also more cost-effective and scalable than MOFs and COFs, which involve complex synthesis processes and expensive precursors. Furthermore, activated carbons demonstrate better chemical and thermal stability compared to conducting polymers, which often experience conductivity loss and mechanical degradation. These factors make activated carbon an ideal choice for reliable, high-performance, and economically viable energy storage systems [18–22].

The pre-carbonization of precursors is a crucial step in the production of activated carbon, as it can significantly affect the final properties of the material. Recognizing its importance, this variable has been the subject of extensive research across various types of precursors. Notably, Kumari et al. [23] conducted a study in which carbon was derived from the incomplete combustion of soybean oil and waste engine oil using the flames of an oil-wick lamp. The resulting carbon was then activated with KOH at 800 °C, producing materials with desirable properties for energy storage in supercapacitors. In a subsequent study, Feng et al. [24] analyzed pre-carbonization at different temperatures, demonstrating that performing pre-carbonization of petroleum coke at elevated temperatures (ranging from 550 to 750 °C) had minimal impact on the properties of the resulting activated carbons. More recently, Deng et al. [25] conducted a study examining the effect of pre-carbonization temperature at lower temperatures (ranging from 400 to 600 °C) using an agricultural precursor to produce activated carbon with KOH for supercapacitor applications. Their findings revealed that the pre-carbonization temperature had a significant influence on the material properties, with 400 °C being identified as the optimal temperature for this precursor.

Although agricultural wastes are the most commonly used for the production of activated carbon, less explored precursors, such as municipal wastes (for instance diapers [26]) or animal-origin wastes, can also be utilized. The pig is an animal widely used to produce various products, which in turn generate waste. Pork is a meat from pig, which is globally consumed in a large quantity. China, USA and European Union are the top 3 highest production of pork globally. In the year 2022, about 34 % of the meat consumed is pork with production capacity of 123 million tons [27]. Approximately 1 billion pigs are raised annually, and several wastes are generated including methane gas, feces, and the hair removed during processing and cleaning. These wastes could find applications as fertilizer, fuel, and production of materials. Interestingly, studies have shown that pig hair contains dietary keratin protein and could be mixed with poultry feed up to 6 % [28]. The use of the pig hair was promoted by its abundance and the nutrient content to balance the amino acid in animal diets. However, the processing as food supplement follows an energy intensive step of conditioning, hydrothermal treatment and purifications.

Pig hair represents a unique and underutilized precursor for the production of activated carbon, offering several distinct advantages for sustainable material development. As an abundant byproduct of the

meat industry, pig hair provides a renewable and cost-effective feedstock that aligns with the principles of waste valorization and circular economy. This approach not only addresses waste management challenges but also contributes to the development of high-performance, eco-friendly energy storage materials.

To date, no studies have been published that specifically investigate the effect of pre-carbonization temperature on the properties of activated carbon derived from animal-origin precursors for use in supercapacitor electrodes. This research gap is particularly significant given the unique characteristics of animal-based materials which can influence the carbonization and activation processes. Beyond the practical benefits highlighted earlier, exploring this aspect offers a critical strategy for optimizing the production of activated carbon. By tailoring the pre-carbonization temperature, it is possible to control the structural and surface properties of the material, thereby enhancing its electrochemical performance. This approach not only contributes to the development of sustainable energy storage materials but also supports the valorization of underutilized industrial byproducts, aligning with global efforts toward waste minimization and circular economy practices.

2. Materials and methods

2.1. Production activated carbon

Pig hair samples were obtained from a slaughterhouse facility. The pig hair was thoroughly washed with hot water and screened to remove any dirt or stones. The characterization of this precursor can be found in Ref. [29]. Briefly, the precursor contains 48.31 % carbon, 5.83 % hydrogen, 4.01 % nitrogen, 0.08 % sulfur, and 41.77 % oxygen, along with 1.77 % ash content and 7.97 % moisture. The cleaned material was then dried and subjected to pre-carbonization at various temperatures (350–500 °C) with a heating rate of 10 °C/min in a fixed-bed reactor. For each experiment, 500 mg of pig hair was processed in a tubular furnace under a high-purity nitrogen atmosphere, with a residence time of 1 h. The resulting pre-carbonized samples were impregnated with KOH at a carbon-to-activating agent ratio of 1:3. Specifically, 15 g of pre-carbonized material were mixed with 45 g of KOH in 150 mL of deionized water and stirred at room temperature for 16 h. After impregnation, the excess water was evaporated by drying the slurry in an oven at 100 °C. The dried sample was then activated in a fixed-bed reactor under a high-purity nitrogen flow (150 mL/min) at 800 °C for 1 h, with a heating rate of 20 °C/min. The chosen activation temperature is supported by previous research which has demonstrated its suitability for the preparation of activated carbon via KOH activation [30–32]. Following activation, the samples were washed with 200 mL of 1 M HCl and rinsed with distilled water until a neutral pH was achieved. The final activated carbon samples were labeled as PH **X**-800, where **X** represents the pre-carbonization temperature.

2.2. Characterization of pig hair carbon

Nitrogen adsorption-desorption isotherms were measured at 77 K using a Quantachrome Nova 2200e physisorption analyzer. Prior to analysis, the samples were degassed at 250 °C for 16 h. The surface area of the samples was calculated using the Brunauer-Emmett-Teller (BET) method, while the pore size distribution was determined using the Quenched Solid Density Functional Theory (QS-DFT) model, analyzed with NovaWin software. Surface morphology was examined through scanning electron microscopy (SEM, Hitachi S-5500) operating at 5 kV, and elemental composition was determined using energy-dispersive X-ray spectroscopy (EDX) integrated with the SEM system, operating at 15 kV. The crystalline phases of the activated carbon samples were characterized using powder X-ray diffraction (XRD) on a Rigaku Ultima IV diffractometer with CuKα radiation. Data were collected over a 2θ range of 10°–70° at a scanning speed of 10°/minute. Raman spectroscopy was performed using a Thermo Scientific spectrometer equipped with a 532 nm laser to further analyze the structural features of the carbon materials.

2.3. Electrochemical performance analysis

The electrochemical performance of the samples was evaluated using a Biologic VMP-300 potentiostat. To prepare the electrode paste, a composition of 80 % pig hair-derived activated carbon, 10 % commercial carbon black (Timcal), and 10 % polytetrafluoroethylene (PTFE) was selected based on preliminary optimization studies. The activated carbon, carbon black, and PTFE were mixed with 10 mL of ethanol and stirred at 60 °C to achieve a homogeneous paste. The mixture was then pressed onto a stainless-steel mesh (1 cm^2) at a pressure of approximately 7 tons. After pressing, the electrodes were dried at room temperature, with an active mass of about 10 mg on each mesh.

For constructing a three-electrode system, pig hair activated carbon served as the working electrode, a graphite rod was the counter electrode, and a saturated sulphate electrode (SSE) was used as the reference. The electrolyte solution was 0.5 M H_2SO_4. The electrochemical properties were characterized by cyclic voltammetry (CV) using various scan rates (5, 10, 20, 40, 60, 80, and 100 mV/s).

$$C_{sp.} = \frac{\int I \cdot dV}{m \cdot \nu \cdot \Delta V} \tag{7}$$

The specific capacitance (*Csp*, in F/g) was calculated based on the integral of the current-voltage curve ($\int IdV$, in A•s), the active mass (m, in grams), the scan rate (ν, in V/s), and the potential window width (ΔV, in volts) according to Equation (7) [33]. Similarly, galvanostatic charge and discharge was used to evaluate the performance of the materials under constant current conditions. The specific capacitance using this technique was calculated as shown in Equation (8) [34].

$$C_{GCD} = \frac{I \cdot t}{m \cdot \Delta V} \tag{8}$$

Where C_{GCD} stands for the specific capacitance in F/g, I is the applied current (A), t is the discharge time (s), m is the active mass (g), and ΔV is the potential window (V). Electrochemical impedance spectroscopy (EIS) was employed to evaluate the real and imaginary components of capacitance for the most effective materials. The measurements were carried out with an amplitude of ±10 mV over a frequency range from 100 kHz to 5 mHz, allowing the calculation of real and imaginary capacitance values, by Equations (9) and (10) [35].

$$C_{Re} = \frac{-Z''(2 \cdot \pi \cdot f)}{2 \cdot \pi \cdot f |Z(2 \cdot \pi \cdot f)|^2} \tag{9}$$

$$C_{Im} = \frac{-Z(2 \cdot \pi \cdot f)}{2 \cdot \pi \cdot f |Z(2 \cdot \pi \cdot f)|^2} \tag{10}$$

Where C_{Re} and C_{im} are the real and imaginary parts of the capacitance (F/g), Z' and Z'' are the real and imaginary contributions of the impedance (Ω), and f is the frequency (Hz). The complex power of the materials was determined through Equations (11) and (12) [36].

$$P = 2 \cdot \pi \cdot f \cdot C_{Im} |\Delta V_{rms}|^2 \tag{11}$$

$$Q = -2 \cdot \pi \cdot f \cdot C_{Re} |\Delta V_{rms}|^2 \tag{12}$$

Where P and Q are the active and reactive power, respectively.

3. Results and discussions

The X-ray diffraction spectra of the four activated carbons produced from pig hair are shown in Fig. 1. All these spectra display the same signals, which appear at approximately 25° and 45° and correspond to

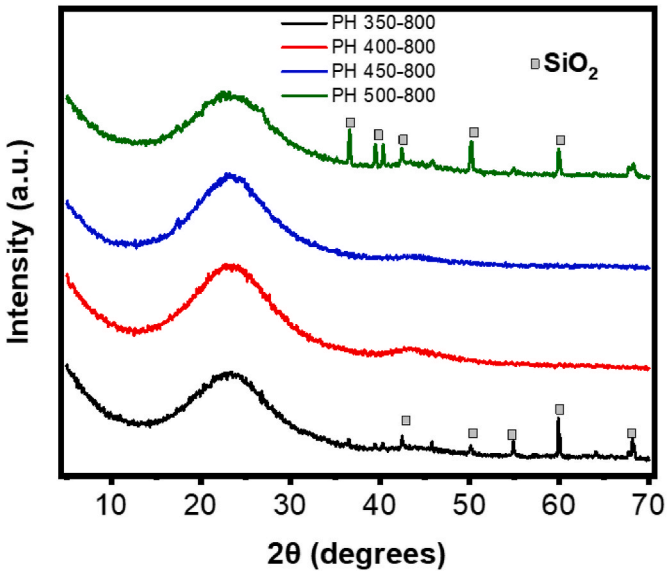

Fig. 1. XRD spectra of pig hair activated carbons.

the (0 0 2) and (1 0 1) planes of graphite. However, the broadness of the peaks indicates that an amorphous structure predominates in all these materials [37]. In addition to these graphite-related responses, traces of silicon oxide (SiO_2) are also observed, which are commonly found in various carbon materials due to the nature of the precursors or the location where they were obtained [38].

To further investigate the structural properties of the materials, Raman analysis of these activated carbons was conducted, yielding the spectra shown in Fig. 2a. These spectra exhibit the typical responses of carbon materials, consistent with the XRD observations, which correspond to two broad peaks observed at approximately 1370 and 1600 cm^{-1} [39].

It is important to highlight that, due to the broadness of the peaks, it can be affirmed that the observed materials are amorphous carbons. Therefore, the observed peaks are a sum of contributions from various overlapping signals. A deconvolution of these signals can be performed to identify the different contributions present. Fig. 2b shows a representative spectrum after its decomposition into five different signals, applying the model reported in Ref. [40]. These identified signals originate from the following bands: Peak I) C-H bonds present in aromatic rings, Peak II) a breathing mode that occurs only in aromatic structures with defects and exhibits A_{1g} symmetry, Peak III) breathing of C-H bonds present in aromatic rings, Peak IV) stretching of sp^2 carbon bonds in aromatic rings, and Peak V) C=O bonds present in the carbon material.

The level of order in the carbon structures can be determined by the ratio between peaks II and IV [41]. In the case of amorphous carbons, a higher ratio, intensity of peak II/intensity of peak IV (II/IV), indicates a greater level of order within the structure. The II/IV ratios for these materials are 2.51, 2.63, 2.68, and 2.71 for PH 350–800, PH 400–800, PH 450–800, and PH 500–800, respectively. This suggests that pre-carbonization prior to activation has the effect of producing more ordered structures as it is carried out at higher temperatures, even though the activation was conducted at the same temperature for all samples.

After confirming the amorphous structure of the materials, their surface structure was examined using microscopy, resulting in the images presented in Fig. 3. It can be observed that all the samples exhibit a porous structure, which is the result of the activation process carried out using KOH. This reagent reacted with the precursor during the thermal treatment, leading to the formation of pores on the surface. When comparing the structures of these materials to assess the effect of carbonization temperature, it is observed that PH 350–800 (Fig. 3a) exhibits a microstructured and compact surface with both porous areas and some regions free of pores. As the carbonization temperature is increased to 400 °C (PH 400–800, Fig. 3b), the pore-free zones become less prevalent, resulting in a more homogeneous surface morphology. In the PH 450–800 material (Fig. 3c), the structure becomes even more porous and less compact. Finally, in PH 500–800 (Fig. 3d), a highly porous, rough structure is evident, indicating that higher carbonization temperatures promote better pore development.

To gain a more detailed understanding of the pore structure, higher magnification images of the sample PH 500–800 were analyzed. At a magnification of 20,000× (Fig. 3e), the pores became more prominent, appearing uniformly distributed across the material's surface. This uniformity suggests a consistent activation process and efficient development of the porous network. When the magnification was increased to 50,000×, additional pores were observed within the channels of the material, revealing a more intricate and interconnected structure. This intricate porosity highlights the material's high surface area, a critical attribute for applications such as energy storage.

The chemical composition of the materials, determined by EDX, is presented in Table 1. As expected, these materials are primarily composed of carbon, with a significant amount of oxygen, which may facilitate energy storage through faradaic processes. Similarly, these materials contain silicon, which is typical for activated carbons derived

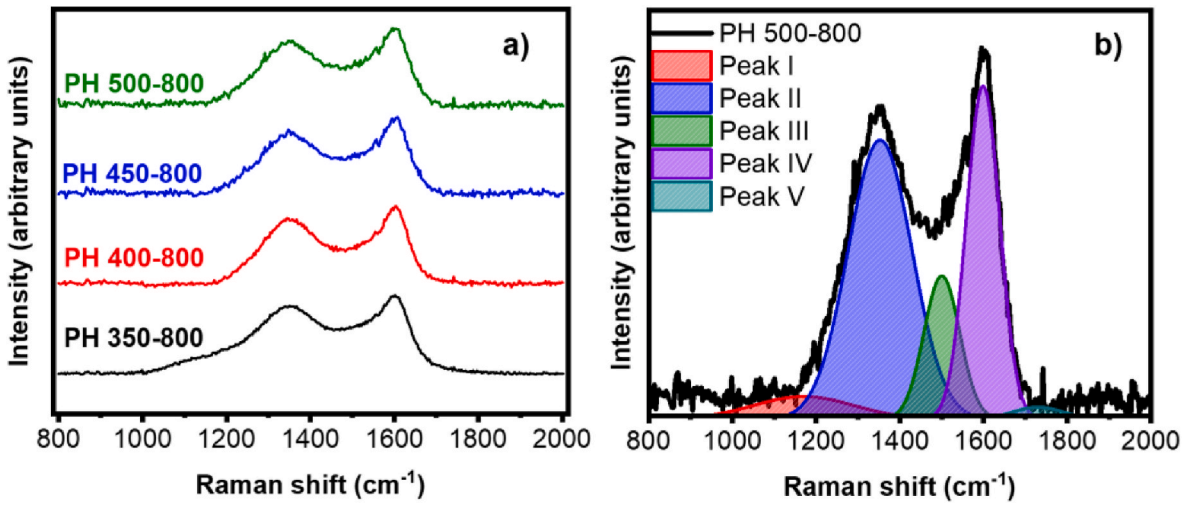

Fig. 2. Raman analysis of pig hair activated carbons. a) Original Raman spectra, b) Representative deconvoluted Raman signal.

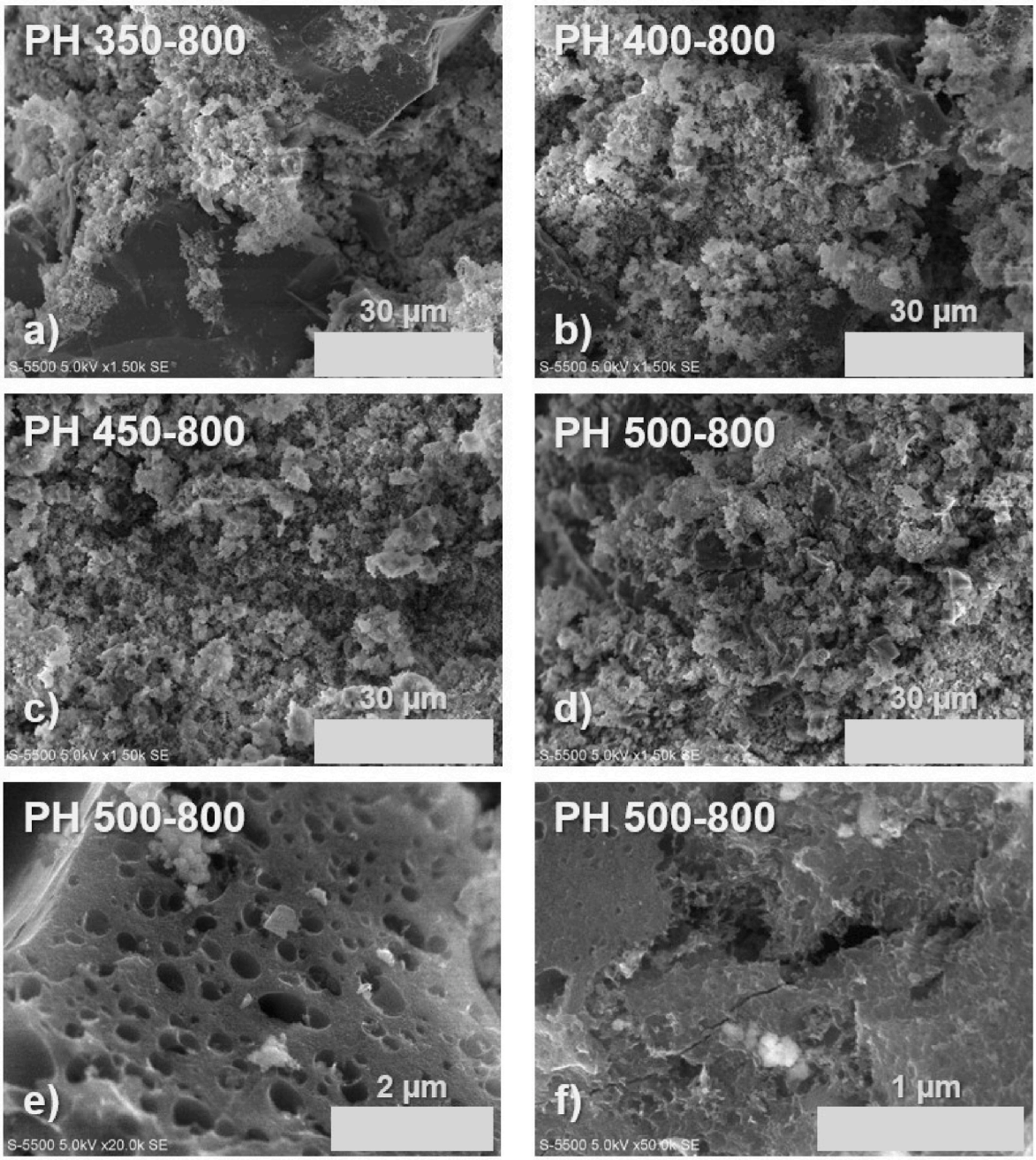

Fig. 3. SEM images of pig hair activated carbons, obtained at 1500 magnifications a) PH 350–800, b) PH 400–800, c) PH 450–800, d) PH 350–800. Detail of PH 500–800 sample at e) 20,000 magnifications, f) 50,000 magnifications.

Table 1
Chemical composition of pig hair activated carbons.

Activated carbon	C (at.%)	O (at.%)	Si (at.%)
PH 350-800	68.05	26.06	5.88
PH 400-800	72.72	21.16	6.12
PH 450-800	55.06	35.81	9.13
PH 500-800	67.72	26.78	5.50

from biomass [42,43].

To quantitatively analyze the porosity, nitrogen physisorption analysis was conducted, and the resulting isotherms are presented in Fig. 4a. According to the latest IUPAC classification [44], these isotherms are a combination of Type I(b)/IV(a), indicating that the materials consist of both micropores (pores smaller than 2 nm) and mesopores (between 2 and 50 nm). Additionally, the increase in adsorption volume at high relative pressures suggests the presence of some macropores (>50 nm). The pore size distribution is presented in Fig. 4b, where it is evident that the materials are predominantly microporous, with pores primarily in the sizes of 0.6 nm and 1.6 nm.

The isotherms also enable the determination of the specific surface area of the materials through the application of adsorption models. Using the Brunauer-Emmett-Teller (BET) model, specific surface areas of 1002 m^2/g for PH 500–800, 795 m^2/g for PH 450–800, 761 m^2/g for PH 400–800, and 117 m^2/g for PH 350–800 were calculated. These differences in surface area account for the varying nitrogen adsorption volumes observed for each sample, indicating that the higher carbonization temperature promoted the development of a larger specific surface area,

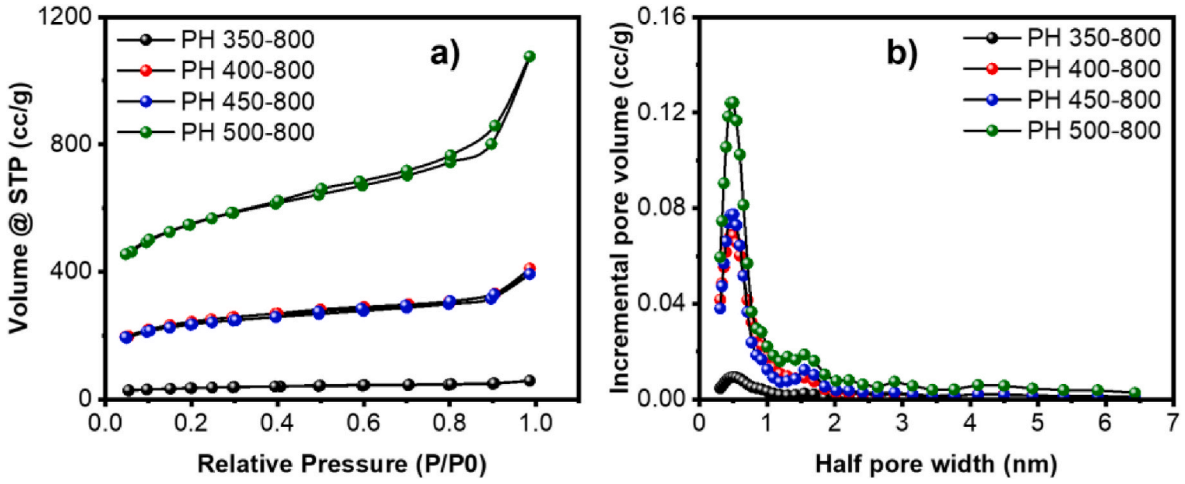

Fig. 4. Nitrogen physisorption analysis of pig hair activated carbons. a) Adsorption/desorption isotherms, b) Pore size distribution.

which correlates with the increased porosity observed in Fig. 3. Comparison of the specific surface areas obtained in this study with those reported in the literature for various precursors reveals that our results are consistent with the expected range [45–48]. This finding suggests that pig hair can be a viable precursor for the production of high surface area materials.

The previously described physicochemical characterization revealed that the pig hair-derived carbons exhibit suitable properties for energy storage. To assess the performance of these materials for this application, voltammetric analysis was first conducted (see Fig. 5). Fig. 5a representatively shows the voltammetric profiles of one of the activated carbons derived from pig hair. It is observed that at lower scan rates, the material exhibits a quasi-rectangular shape, characteristic of electrical double layer storage [49]. This indicates that electrolyte ions accumulate on the electrode surface through electrostatic attractions [50]. Additionally, some distortions in the profile are noted as the scan rate increases. These distortions are attributed to the ions having less time to penetrate the pores of the material, leading to mass transport resistance. Similarly, the deviation from a perfect rectangular profile on the electrode suggests that the active material is also undergoing charge transfer processes, i.e., chemical reactions, which can be attributed to the presence of oxygen detected on the surface [51].

A comparison of the profiles of the four activated carbons derived from pig hair is presented in Fig. 5b. This figure shows that all these materials exhibit similar electrochemical profiles, though with different current intensities. The difference in current intensities indicates that the materials store varying amounts of energy, which can be primarily attributed to the difference in specific surface area due to the porosity of the materials. In other words, materials with a higher specific surface area have more space to accommodate a larger number of ions in their structure [52], making PH 500–800 the material with the highest current intensity. In quantitative terms, the specific capacitance of these materials is presented in Fig. 5c. The specific capacitance shown here is directly proportional to the current intensity and, consequently, to the number of ions stored on the material's surface. The descending order of capacitance among the materials is as follows: PH 500–800, PH 450–800, PH 400–800, and PH 350–800 being 110, 84, 80 and 41 F/g, respectively at the lowest scan rate (5 mV/s). These capacitances decrease to 52, 46, 38 and 22 F/g at the highest scan rate. This indicates that the carbonization temperature prior to chemical activation is directly proportional to the capacitance of the materials.

As previously mentioned, the total capacitance is the sum of contributions from the electric double layer (an electrostatic process) and from faradaic charge transfer processes. Both contributions can be identified using the model proposed by Dunn et al. [53]. Fig. 6 shows the deconvolution for the best-performing material (PH 500–800) and the material with the lowest specific capacitance (PH 350–800), at a scan rate of 20 mV/s. This figure reveals that the primary contribution of the materials to energy storage comes from the electric double layer, which accounts for its superior performance compared to the other materials. Additionally, there is a significant contribution from faradaic processes, mainly attributed to the functional groups present in these materials, being slightly higher for PH 350–800. Based on what is observed in this figure, the pre-carbonization temperature does not have a significant influence on the contributions to the total capacitance in these activated carbons.

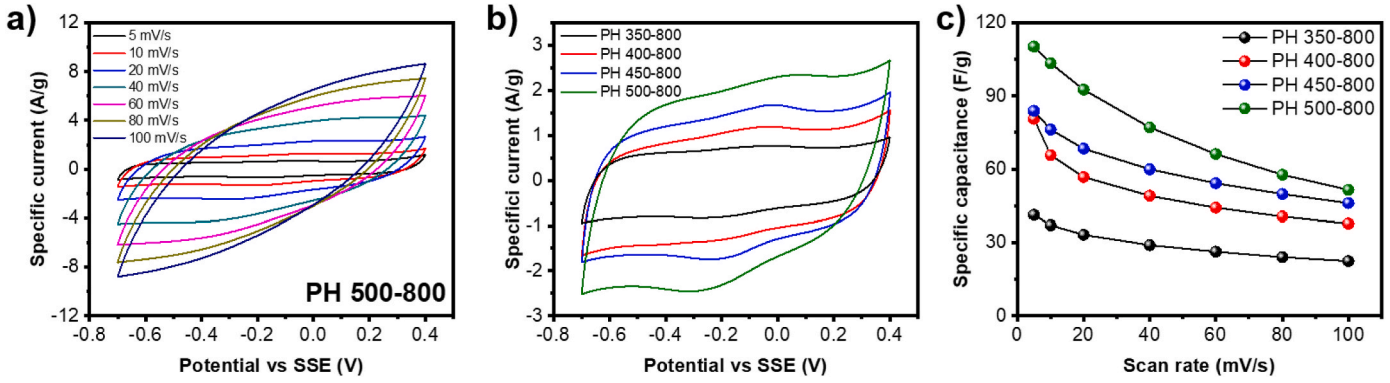

Fig. 5. Analysis of pig hair activated carbons through cyclic voltammetry. A) Representative voltammogram at different scan rates, b) Comparative cyclic voltammograms at 20 mV/s, c) Specific capacitance vs scan current.

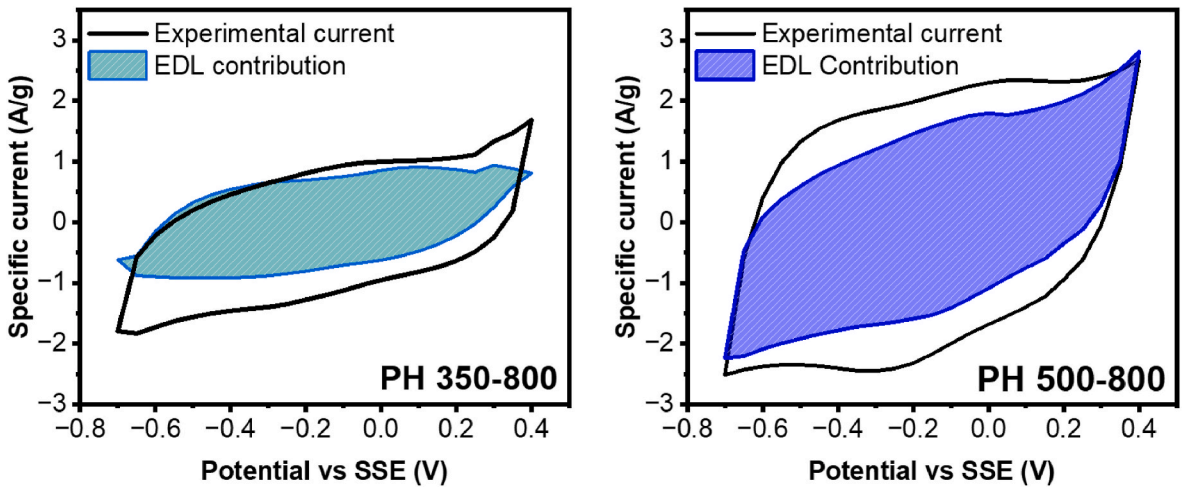

Fig. 6. Deconvoluted cyclic voltammograms of the pig hair activated carbon with the highest and lowest specific capacitance.

Similarly, the behavior of these carbon materials was also evaluated using the galvanostatic charge-discharge technique (Fig. 7), where the materials are charged and discharged at a constant current. Fig. 7a representatively shows the charge-discharge profiles of the PH 500–800 material at various applied currents. It can be observed that as the current intensity increases, the cycling time becomes shorter, allowing less time for the ions to accumulate on the material's surface.

The comparison between the charge-discharge profiles is shown in Fig. 7b, where the charge and discharge times exhibit a direct proportionality to the carbonization temperature, in good agreement with the cyclic voltammetry results. Similarly, the profiles display a semi-rectangular shape, which again indicates that the primary energy storage mechanism is through the electric double layer, as also suggested by Fig. 6. The same trend observed in Fig. 5c is reflected in the specific capacitances determined through GCD, as shown in Fig. 7c, with PH 500–800 being the most capacitive material and PH 350–800 the least capacitive.

Electrochemical impedance spectroscopy analysis allows for the determination of resistive parameters and complex behavior (in the real and imaginary planes) of electrodes made of activated carbons [54]. Fig. 8a presents a representative Nyquist plot for these materials, where the impedances are shown on the real axis (resistance) and the imaginary axis (reactance). The profile exhibited by this material aligns with the expected behavior of a supercapacitor. Initially, a semicircle appears at high frequencies (see inset in Fig. 8a), which represents the intrinsic resistance due to system connections (first intersection with the real axis) as well as the resistance at the electrode/electrolyte interface (diameter of the semicircle). Subsequently, at intermediate frequencies, a region showing a combination of resistive and capacitive behavior is observed as an inclined line. Finally, at the lowest frequencies, there is sufficient time for ions dissolved in the electrolyte to properly penetrate the pores of the material, resulting in capacitive behavior, which is typically represented as a vertical line in the Nyquist plot.

The capacitive behavior observed through electrochemical impedance spectroscopy can be calculated across any portion of the material's potential window, as illustrated in Fig. 8b. As shown, the profile obtained by calculating capacitance using this technique mirrors the shape of the profiles determined via cyclic voltammetry, thereby validating the results obtained by both methods. Similarly, the trend in capacitance values aligns with those observed through cyclic voltammetry and galvanostatic charge-discharge, reaffirming for the third time that the carbonization temperature is directly proportional to the material's specific capacitance.

Analyzing the complex behavior of the material is crucial for understanding its response to alternating current. Fig. 9a,d displays the real and imaginary components of capacitance. The real capacitance reflects the material's ability to store energy in a supercapacitor, while the imaginary capacitance represents energy losses in the form of heat [36]. At high frequencies, the materials do not exhibit any of these capacitances, as the behavior is purely resistive, as seen in the Nyquist plot. Conversely, as the frequency decreases, both capacitances tend to increase, although not in the same manner; the real capacitance continuously rises until it reaches a value similar to that determined through cyclic voltammetry and galvanostatic charge-discharge, being

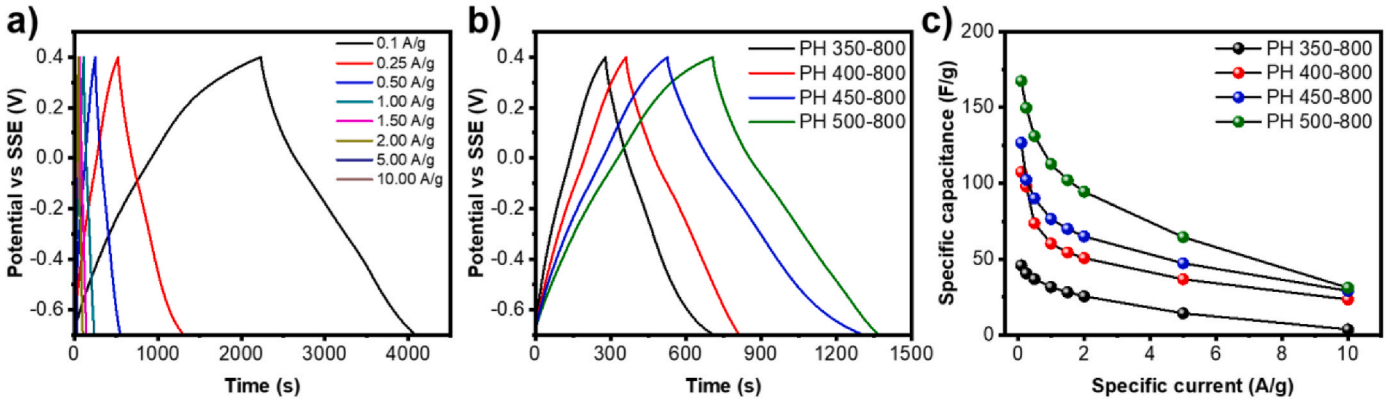

Fig. 7. Analysis of pig hair activated carbons through GCD. A) Representative GCD profiles at different specific currents, b) Comparative GCD profiles at 0.5 A/g, c) Specific capacitance vs applied current.

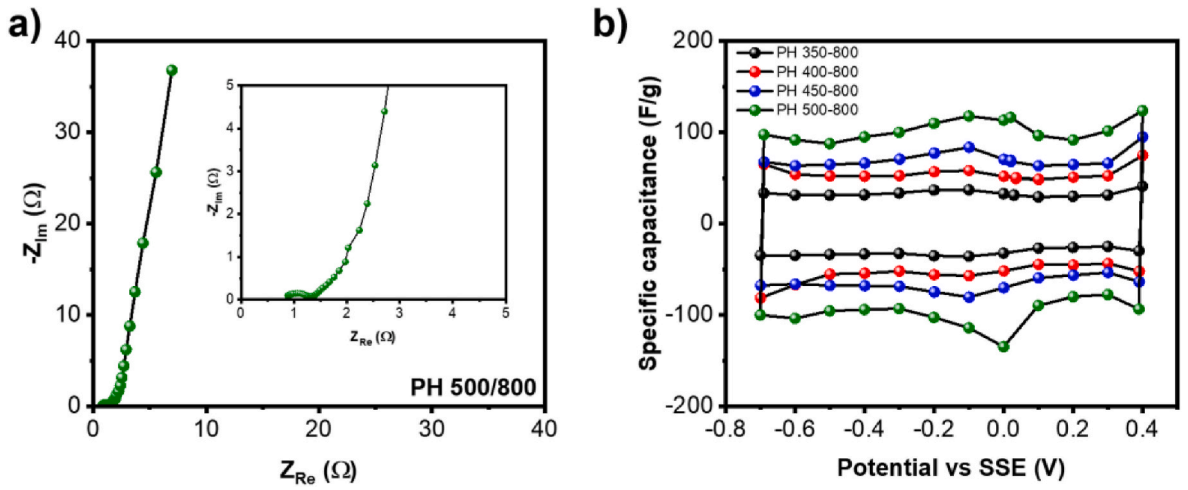

Fig. 8. Impedance analysis of pig hair activated carbons. a) Representative Nyquist plot, b) Specific capacitance calculated at different potentials.

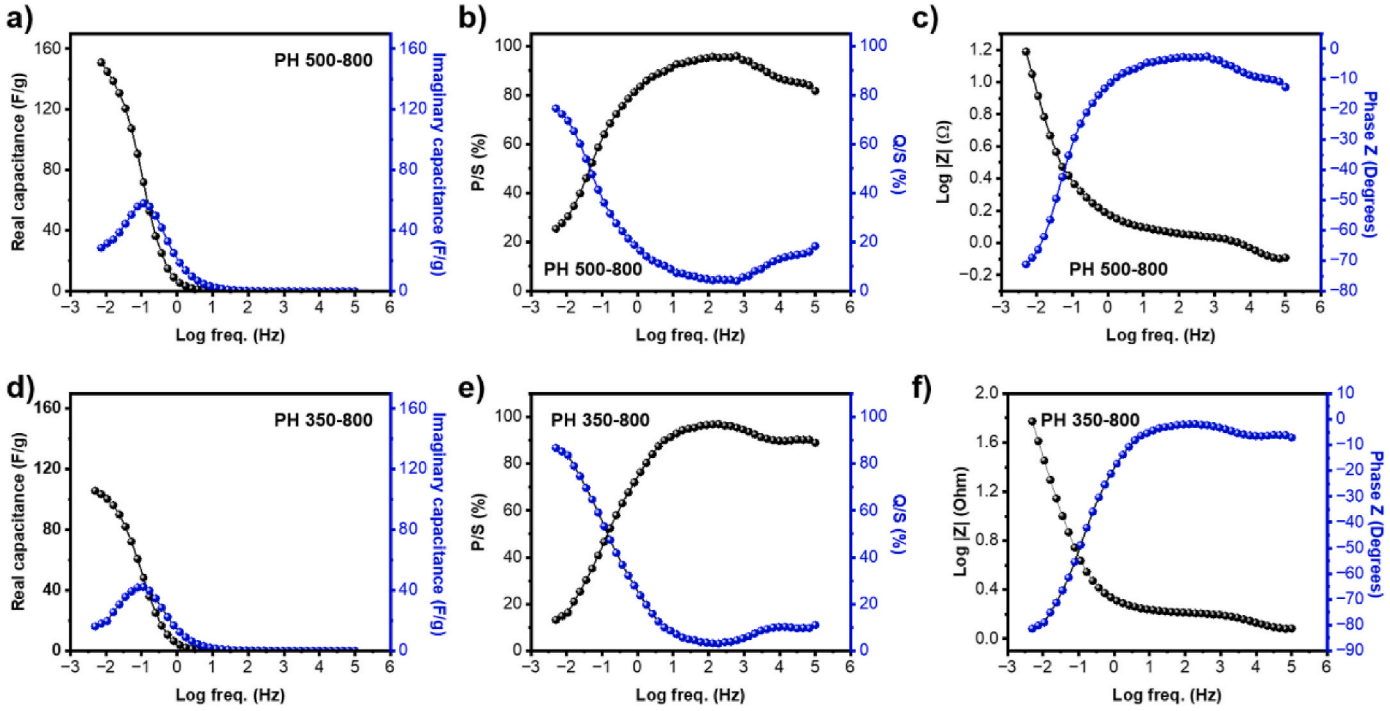

Fig. 9. Complex behavior of PH 500–800 & PH 350–800 activated carbons. a,d) Complex capacitance, b,e) Complex power, c,f) Bode plot.

higher for PH 500–800 than for PH 350–800. In contrast, the imaginary capacitance increases until it reaches a peak, which corresponds to the frequency at which capacitive and resistive contributions are balanced, and then decreases as the frequency continues to drop.

The complex behavior is also illustrated in the power response (Fig. 9b,e). In this graphs, P/S represents the normalized real power contribution, while Q/S represents the normalized reactive power contribution. At high frequencies, when the materials act as a resistor, the real power (P/S) tends to be dissipated almost entirely (which only occurs in an ideal system). Conversely, as the frequency decreases, the material predominantly exhibits reactive power (Q/S), which is the expected behavior for a supercapacitor [36].

Finally, Fig. 9c,f presents the Bode plots for PH 500–800 and PH 350–800. These diagrams simultaneously show the change in the magnitude of impedance and the phase angle with respect to frequency. These two variables intersect. In an ideal double-layer capacitor, this intersection occurs at a phase angle of 45°; however, since these materials also exhibits faradaic processes, the angles are slightly shifted to −39° for PH 500–800 and to −52° for PH 350–800. The frequency at which this crossover occurs is known as the characteristic frequency, and the inverse of its magnitude represents the shortest time in which the material can discharge while delivering at least 50 % of its energy as electricity [55]. In this particular case, the time corresponds to 15.6 s, indicating the high power of PH 500–800, and 45.5 s for PH 350–800 indicating a lower power for this material.

4. Conclusions

This study represents the first investigation into the effect of pre-carbonization at temperatures of 350, 400, 450, and 500 °C on the energy storage properties of activated carbons derived from pig hair, a sustainable and abundant precursor. Potassium hydroxide was

employed as the activating agent to create materials suitable for application as supercapacitor electrodes. The pre-carbonization process was found to play a pivotal role in determining the structural and electrochemical properties of the resulting activated carbons. Higher pre-carbonization temperatures yielded materials with a greater degree of structural order, larger surface areas, and enhanced conductivity. These attributes directly contributed to improved energy storage performance, primarily through electric double-layer capacitance, by providing more accessible surface area for ion adsorption and charge accumulation. In addition to the observed capacitive behavior, the presence of oxygen-containing functional groups imparted by the precursor contributed significantly to faradaic processes, further enhancing the energy storage capacity of the materials. This synergistic effect underscores the importance of optimizing pre-carbonization conditions to balance structural and chemical properties for superior electrode performance. Finally, this study demonstrates that pre-carbonization under controlled conditions is a crucial step in the production of high-performance activated carbons from animal-origin precursors. The findings provide valuable insights into the development of sustainable materials with enhanced energy storage properties, paving the way for eco-friendly advancements in supercapacitor technology.

CRediT authorship contribution statement

Diego Ramón Lobato-Peralta: Writing – original draft, Validation, Methodology, Investigation, Formal analysis, Data curation, Conceptualization. **Jude A. Okolie:** Investigation, Data curation. **Henry O. Orugba:** Visualization, Conceptualization. **D.M. Arias:** Formal analysis, Conceptualization. **P.J. Sebastian:** Validation, Supervision, Conceptualization. **Patrick U. Okoye:** Writing – review & editing, Validation, Supervision, Resources, Data curation, Conceptualization.

Acknowledgements

The authors of this work gratefully acknowledge Rogelio Morán Elvira for the technical support for SEM & EDS, and María Luisa Ramón García for XRD. This work was financially supported by Dirección General de Asuntos del Personal Académico, México under Programa de Apoyo a Proyectos de Investigación e Innovación Tecnológica (DGAPA-PAPIIT) Project Number IN109725.

Data availability

Data will be made available on request.

References

[1] D.R. Lobato-Peralta, P.U. Okoye, C. Alegre, A review on carbon materials for electrochemical energy storage applications: state of the art, implementation, and synergy with metallic compounds for supercapacitor and battery electrodes, J. Power Sources 617 (2024), https://doi.org/10.1016/j.jpowsour.2024.235140.

[2] K. Dissanayake, D. Kularatna-Abeywardana, A review of supercapacitors: materials, technology, challenges, and renewable energy applications, J. Energy Storage 96 (2024), https://doi.org/10.1016/j.est.2024.112563.

[3] Z.U. Khan, J. Jiang, M.Y.A. Khan, A comprehensive review on recent advancements in new carbon and metal-organic framework base energy storage materials and devices, J. Energy Storage 100 (2024), https://doi.org/10.1016/j.est.2024.113464.

[4] S. Raza, A. Hayat, T. Bashir, C. Chen, L. Shen, Y. Orooji, H. Lin, Electrochemistry of 2D-materials for the remediation of environmental pollutants and alternative energy storage/conversion materials and devices, a comprehensive review, Sustainable Materials and Technologies 40 (2024), https://doi.org/10.1016/j.susmat.2024.e00963.

[5] B.K. Chakrabarti, C.T.J. Low, Scaling to practical pouch cell supercapacitor: electrodes by electrophoretic deposition, Next Energy 4 (2024) 100137, https://doi.org/10.1016/j.nxener.2024.100137.

[6] C. Zhang, N. Chen, M. Zhao, W. Zhong, W.J. Wu, Y. can Jin, High-performance electrode materials of heteroatom-doped lignin-based carbon materials for supercapacitor applications, Int. J. Biol. Macromol. 273 (2024), https://doi.org/10.1016/j.ijbiomac.2024.133017.

[7] N.A.M. Barakat, M.S. Mahmoud, H.M. Moustafa, Comparing specific capacitance in rice husk-derived activated carbon through phosphoric acid and potassium hydroxide activation order variations, Sci. Rep. 14 (2024), https://doi.org/10.1038/s41598-023-49675-0.

[8] A. Sandeep, P. T, A.V. Ravindra, Activated carbon derived from corncob via hydrothermal carbonization as a promising electrode for supercapacitors, Mater. Res. Bull. 179 (2024), https://doi.org/10.1016/j.materresbull.2024.112991.

[9] Y. Gao, C. Liu, Y. Jiang, Y. Zhang, Y. Wei, G. Zhao, R. Liu, Y. Liu, G. Shi, G. Wang, Hydrothermal assisting biomass into a porous active carbon for high-performance supercapacitors, Diam. Relat. Mater. 148 (2024), https://doi.org/10.1016/j.diamond.2024.111487.

[10] M. Zimik, S. Sarmah, B.K. Kakati, D. Deka, R. Thangavel, Pyrolytic conversion of Mesua ferrea testa to nitrogen-doped porous carbon for supercapacitor applications, Mater. Res. Bull. 180 (2024), https://doi.org/10.1016/j.materresbull.2024.113017.

[11] V. Kavan Kumar, N.L. Panwar, A review on porous carbon synthesis processes and its application as energy storage supercapacitor, J. Indian Chem. Soc. 101 (2024), https://doi.org/10.1016/j.jics.2024.101231.

[12] N. Boonraksa, E. Swatsitang, K. Wongsaprom, Biomass nanoarchitectonics with activated rice husk char for nanoporous carbon as electrode material: enhancing supercapacitor electrochemical performance, J. Non-Cryst. Solids 637 (2024), https://doi.org/10.1016/j.jnoncrysol.2024.123064.

[13] D.R. Lobato-Peralta, A. Ayala-Cortés, A. Longoria, D.E. Pacheco-Catalán, P. U. Okoye, H.I. Villafán-Vidales, C.A. Arancibia-Bulnes, A.K. Cuentas-Gallegos, Activated carbons obtained by environmentally friendly activation using solar energy for their use in neutral electrolyte supercapacitors, J. Energy Storage 52 (2022), https://doi.org/10.1016/j.est.2022.104888.

[14] F. Niaz, S.S. Shah, K. Hayat, M.A. Aziz, G. Liu, Y. Iqbal, M. Oyama, Utilizing rubber plant leaf petioles derived activated carbon for high-performance supercapacitor electrodes, Ind. Crops Prod. 219 (2024), https://doi.org/10.1016/j.indcrop.2024.119161.

[15] S. Subraya Hegde, B. Ramachandra Bhat, Impact of electrolyte concentration on electrochemical performance of Cocos nucifera Waste-Derived High-Surface carbon for green energy storage, Fuel 371 (2024), https://doi.org/10.1016/j.fuel.2024.131999.

[16] S.S. Hegde, B.R. Bhat, Biomass waste-derived porous graphitic carbon for high-performance supercapacitors, J. Energy Storage 76 (2024), https://doi.org/10.1016/j.est.2023.109818.

[17] S.S. Hegde, B.R. Bhat, Sustainable energy storage: mangifera indica leaf waste-derived activated carbon for long-life, high-performance supercapacitors, RSC Adv. 14 (2024) 8028–8038, https://doi.org/10.1039/d3ra08910j.

[18] P. Adoor, S.S. Hegde, B.R. Bhat, S.D. George, R. Yeenduguli, Electrochemical performance and structural evolution of spray pyrolyzed Mn_3O_4 thin films in different aqueous electrolytes: effect of anions and cations, RSC Adv. 14 (2024) 29748–29762, https://doi.org/10.1039/D4RA05426A.

[19] P. Adoor, S.S. Hegde, B.R. Bhat, S.N. Yethadka, R. Yeenduguli, Elucidating the role of copper-induced mixed phases on the electrochemical performance of Mn-based thin-film electrodes, ACS Omega 8 (2023) 46640–46652, https://doi.org/10.1021/acsomega.3c05614.

[20] A. Pramitha, S.S. Hegde, B.R. Bhat, S.D. George, Y.N. Sudhakar, Y. Raviprakash, Properties of Mn3O4 thin film electrodes prepared using spray pyrolysis for supercapacitor application, Mater. Chem. Phys. 307 (2023), https://doi.org/10.1016/j.matchemphys.2023.128213.

[21] A. Pramitha, S.S. Hegde, B. Ramachandra Bhat, C. Yadav K, S. Chakraborty, A. Ravikumar, S.D. George, Y.N. Sudhakar, Y. Raviprakash, Unveiling the mass-loading effect on the electrochemical performance of Mn3O4 thin film electrodes: a combined computational and experimental study, Phys. Scripta 99 (2024), https://doi.org/10.1088/1402-4896/ad7206.

[22] N.P. Agadi, S.S. Hegde, N.L. Teradal, B.R. Bhat, J. Seetharamappa, Unveiling the versatile applications of cobalt oxide-embedded nitrogen-doped porous graphene for enhanced energy storage and simultaneous determination of ascorbic acid, dopamine and uric acid, J. Electrochem. Soc. 171 (2024) 097510, https://doi.org/10.1149/1945-7111/ad798d.

[23] R. Kumari, S. Kumar Sharma, V. Singh, C. Ravi Kant, Facile, two-step synthesis of activated carbon soot from used soybean oil and waste engine oil for supercapacitor electrodes, in: Mater Today Proc, Elsevier Ltd, 2022, pp. 483–489, https://doi.org/10.1016/j.matpr.2022.07.253.

[24] H. Feng, T. Zhou, L. Ge, Q. Li, C. Zhao, J. Huang, Y. Wang, Study on the preparation of high value-added activated carbon from petroleum coke: comparison between one- and two-step methods for carbonization and activation, Energy 292 (2024), https://doi.org/10.1016/j.energy.2024.130570.

[25] L. Deng, Y. Zhao, S. Sun, D. Feng, W. Zhang, Preparation of corn straw-based carbon by "carbonization-KOH activation" two-step method: gas–solid product characteristics, activation mechanism and hydrogen storage potential, Fuel 358 (2024), https://doi.org/10.1016/j.fuel.2023.130134.

[26] C. Giovanni-Mondragón, D.R. Lobato-Peralta, J.A. Okolie, D.M. Arias, H. O. Orugba, P.J. Sebastian, P.U. Okoye, Electrochemical hydrogen storage in high surface area microporous carbon from disposable diaper waste, Int. J. Hydrogen Energy 50 (2024) 1369–1380, https://doi.org/10.1016/j.ijhydene.2023.09.239.

[27] FAO, Production: crops and livestock products, in: FAOSTAT. Rome, 2023.

[28] J.D. Summers, S. Leeson, UTILIZATION OF PROCESSED PIG HAIR IN POULTRY DIETS, 1978.

[29] H.O. Orugba, J.E. Sinebe, J.L. Chukwuneke, V.I. Okoro, C.L. Enyi, O.I. Ani, Adsorption of cadmium from wastewater with activated carbons derived from pig fur biowaste: A comparative study of in-situ and ex-situ activation routes, Heliyon 10 (2024) 12345, https://doi.org/10.1016/j.heliyon.2024.e37768.

[30] J. Wang, S. Lei, L. Liang, Preparation of porous activated carbon from semi-coke by high temperature activation with KOH for the high-efficiency adsorption of

aqueous tetracycline, Appl. Surf. Sci. 530 (2020), https://doi.org/10.1016/j.apsusc.2020.147187.
[31] X. Cui, Y. Jiang, Z. He, Z. Liu, X. Yang, J. Wan, Y. Liu, F. Ma, Preparation of tank-like resin-derived porous carbon sphere for supercapacitor: the influence of KOH activator and activation temperature on structure and performance, Diam. Relat. Mater. 136 (2023), https://doi.org/10.1016/j.diamond.2023.110054.
[32] Y. Mi, W. Wang, S. Zhang, Y. Guo, Y. Zhao, G. Sun, Z. Cao, Ultra-high specific surface area activated carbon from Taihu cyanobacteria via KOH activation for enhanced methylene blue adsorption, Chin. J. Chem. Eng. 67 (2024) 106–116, https://doi.org/10.1016/j.cjche.2023.12.002.
[33] A. Jain, M. Ghosh, M. Krajewski, S. Kurungot, M. Michalska, Biomass-derived activated carbon material from native European deciduous trees as an inexpensive and sustainable energy material for supercapacitor application, J. Energy Storage 34 (2021), https://doi.org/10.1016/j.est.2020.102178.
[34] P. Saha, N.C.D. Nath, M.M. Islam, M.A. Aziz, A.J.S. Ahammad, Recent progress of high-energy density supercapacitors based on nanostructured nickel oxides, Electrochim. Acta 504 (2024), https://doi.org/10.1016/j.electacta.2024.144892.
[35] P. Navalpotro, M. Anderson, R. Marcilla, J. Palma, Insights into the energy storage mechanism of hybrid supercapacitors with redox electrolytes by Electrochemical Impedance Spectroscopy, Electrochim. Acta 263 (2018) 110–117, https://doi.org/10.1016/j.electacta.2017.12.167.
[36] P.L. Taberna, P. Simon, J.F. Fauvarque, Electrochemical characteristics and impedance spectroscopy studies of carbon-carbon supercapacitors, J. Electrochem. Soc. 150 (2003) A292, https://doi.org/10.1149/1.1543948.
[37] Y. Niu, Q. Fang, X. Zhang, J. Zhao, Y. Li, Structural evolution, induced effects and graphitization mechanism of reduced graphene oxide sheets/polyimide composites, Compos. B Eng. 134 (2018) 127–132, https://doi.org/10.1016/j.compositesb.2017.09.047.
[38] J. Muñiz, A.K. Cuentas-Gallegos, M. Robles, A. Guillén-López, D.R. Lobato-Peralta, J.E. Pascoe-Sussoni, Lignin-derived materials for supercapacitors, in: R. Boddula, A. Khan, A.M. Asiri, A.E. Kolosov (Eds.), Handbook of Supercapacitor Materials, first ed., Wiley-VCH, 2022, 978-3-527-34687-5.
[39] A.C. Ferrari, Raman spectroscopy of graphene and graphite: disorder, electron-phonon coupling, doping and nonadiabatic effects, Solid State Commun. 143 (2007) 47–57, https://doi.org/10.1016/j.ssc.2007.03.052.
[40] D.R. Lobato-Peralta, C.E. Arreola-Ramos, A. Ayala-Cortés, D.E. Pacheco-Catalán, M. Robles, A. Guillén-López, J. Muñiz, P.U. Okoye, H.I. Villafán-Vidales, C. A. Arancibia-Bulnes, A.K. Cuentas-Gallegos, Optimizing capacitance performance: solar pyrolysis of lignocellulosic biomass for homogeneous porosity in carbon production, J. Clean. Prod. 448 (2024), https://doi.org/10.1016/j.jclepro.2024.141622.
[41] A. Ferrari, J. Robertson, Interpretation of Raman spectra of disordered and amorphous carbon, Phys. Rev. B Condens. Matter 61 (2000) 14095–14107, https://doi.org/10.1103/PhysRevB.61.14095.
[42] F. Niaz, S.S. Shah, K. Hayat, M.A. Aziz, G. Liu, Y. Iqbal, M. Oyama, Utilizing rubber plant leaf petioles derived activated carbon for high-performance supercapacitor electrodes, Ind. Crops Prod. 219 (2024), https://doi.org/10.1016/j.indcrop.2024.119161.
[43] N. Chaiammart, V. Vignesh, M.M. Thu, A. Eiad-ua, T. Maiyalagan, G. Panomsuwan, Chemically activated carbons derived from cashew nut shells as potential electrode materials for electrochemical supercapacitors, Carbon Resources Conversion (2024), https://doi.org/10.1016/j.crcon.2024.100267.
[44] M. Thommes, K. Kaneko, A.V. Neimark, J.P. Olivier, F. Rodriguez-Reinoso, J. Rouquerol, K.S.W. Sing, Physisorption of gases, with special reference to the evaluation of surface area and pore size distribution (IUPAC Technical Report), Pure Appl. Chem. 87 (2015) 1051–1069, https://doi.org/10.1515/pac-2014-1117.
[45] A.R. Karim, M. Danish, M.G. Alam, T.G. Seng, Effect of different ratio KOH treatment on neem bark in the formation of activated carbon: adsorption characteristics study, Surface. Interfac. 55 (2024), https://doi.org/10.1016/j.surfin.2024.105476.
[46] C.E. Sánchez-Rodríguez, E. Tovar-Martínez, R. López-Sandoval, Oxidative calcination-enhanced KOH activation of D-glucose-derived carbon spheres for high microporosity in supercapacitor electrodes, Electrochim. Acta 507 (2024), https://doi.org/10.1016/j.electacta.2024.145151.
[47] N. Zhao, Y. Feng, M. Xiong, P. Fu, Renewable biomass bougainvillea petals-derived porous carbon through KOH activation and B/N co-doping: synergistic contribution and charge storage mechanism, Appl. Surf. Sci. 672 (2024), https://doi.org/10.1016/j.apsusc.2024.160852.
[48] G. Zhang, G. Wu, J. Li, Y. Wang, S. Xu, X. Niu, R. Wu, J. Jiang, D. John Blackwood, J. Song Chen, KOH-activated hollow carbon spheres with surface functionalization for high-capacity and long-cycle-life lithium-selenium batteries, J. Colloid Interface Sci. 674 (2024) 852–861, https://doi.org/10.1016/j.jcis.2024.06.212.
[49] Y. Yu, W. Qin, C. Zheng, X. Ding, Z. Li, X. Cao, Y. Wang, Mangosteen husk-derived porous carbon for quasi solid-state supercapacitor with advanced performances, Mater. Lett. 376 (2024) 137316, https://doi.org/10.1016/j.matlet.2024.137316.
[50] Y.R. Lin, Y.K. Hwang, K.K. Chan, C.L. Wu, J.Z. Chen, F.C. Chang, Lignosulfonate-derived porous carbon via self-activation for supercapacitor electrodes, Ind. Crops Prod. 221 (2024), https://doi.org/10.1016/j.indcrop.2024.119330.
[51] F. Lu, W. Kong, K. Su, P. Xia, Y. Xue, X. Zeng, X. Wang, M. Zhou, Activating the pseudocapacitance of multiple-doped carbon foam via long-term charge-discharge circulation, Chem. Eng. Sci. 265 (2023), https://doi.org/10.1016/j.ces.2022.118232.
[52] M. Zimik, S. Sarmah, B.K. Kakati, D. Deka, R. Thangavel, Pyrolytic conversion of Mesua ferrea testa to nitrogen-doped porous carbon for supercapacitor applications, Mater. Res. Bull. 180 (2024), https://doi.org/10.1016/j.materresbull.2024.113017.
[53] J. Wang, J. Polleux, J. Lim, B. Dunn, Pseudocapacitive contributions to electrochemical energy storage in TiO 2 (anatase) nanoparticles, J. Phys. Chem. C 111 (2007) 14925–14931, https://doi.org/10.1021/jp074464w.
[54] D.R. Lobato-Peralta, A. Ayala-Cortés, A. Longoria, D.E. Pacheco-Catalán, P. U. Okoye, H.I. Villafán-Vidales, C.A. Arancibia-Bulnes, A.K. Cuentas-Gallegos, Activated carbons obtained by environmentally friendly activation using solar energy for their use in neutral electrolyte supercapacitors, J. Energy Storage 52 (2022), https://doi.org/10.1016/j.est.2022.104888.
[55] D.R. Lobato-Peralta, D.E. Pacheco-Catalán, P.E. Altuzar-Coello, F. Béguin, A. Ayala-Cortés, H.I. Villafán-Vidales, C.A. Arancibia-Bulnes, A.K. Cuentas-Gallegos, Sustainable production of self-activated bio-derived carbons through solar pyrolysis for their use in supercapacitors, J. Anal. Appl. Pyrolysis 150 (2020), https://doi.org/10.1016/j.jaap.2020.104901.